Monitoring of water imbibition of a particular porous pavement structure by impulse and step-frequency radar

Xavier Dérobert, Amine Ihamouten, F. Bosc, D. Guilbert, J.N. Gaudin, S. Todkar, F. Bernardin, J.L. Bicard

Monitoring of water imbibition of a particular porous pavement structure by impulse and step-frequency radar

Dérobert X.
IFSTTAR
Bouguenais, France
xavier.derobert@ifsttar.fr

Ihamouten A., Bosc F., Guilbert D., Gaudin J.N., Todkar S.
DTer Ouest
CEREMA
Clermont-Ferrand, France
amine.ihamouten@cerema.fr

Bernardin F., *Bicard J.L.*
DTer Centre-Est
CEREMA
Clermont-Ferrand, France
frederic.bernardin@cerema.fr

***Abstract*—Ground-penetrating and step-frequency radar (GPR & SFR) were performed on a particular porous pavement structure. This pavement test site was designed in the frame of a general research on energy storage, using capture solar energy, for deicing road in winter. The objective herein is to monitor water imbibition at the early stage in the pavement to estimate the fluid transfer.**

Amplitudes and travel times, processed from GPR Bscans measurements, are studied and discussed in association to full wave-form inversion (FWFI), used on static SFR measurements which enable to give quantitative information. GPR picking and SFR inversion results are commented and compared during a complete imbibition process.

Keywords—GPR, step-frequency radar; full-wave form inversion; pavement; water imbibition

I. INTRODUCTION

In the frame of climate change and road designs promoting economical and environment-friendly maintenance, successful anti-icing road structures are studied. Their principle is to use asphalt pavement

as an energy source, in order to prevent the formation of ice and snow on roads by storing the captured solar energy at the road during hot periods in order to use it during cold periods.A successful anti-icing economical and environment-friendly techniques are needed to increase road safety and mobility. For these reasons, research has been started recently in order to study alternative procedures to prevent the formation of ice and snow on roads by storing the captured solar energy at the road during hot periods in order to use it during cold periods.

Various innovations have been studied to use asphalt pavement as an energy source [1, 2], the latter ones focused on asphalt solar collectors [3]. The study herein focus on other concept of heat exchanger installations based on the use of drainage asphalt in the bonding layer through which a heated fluid flows via gravity to deice the roadway [4]. So, a full-scale experimental test site was designed to test the various technologies, from the supply of heat transfer fluid, the heat transfer behavior through the pavement structure to the geothermal storage.

To better fit the modeling of the thermal fluid flow to experiments, non-destructive testing (NDT) were performed on this test site using Ground-penetrating radar (GPR). This high efficiency NDT technique, widely used in civil engineering [5], enable to give accurate geometrical information especially for pavement investigation [6,7].

The study herein focused on water imbibition at the early stage in the pavement structure by GPR to estimate the velocity of the fluid transfer. A complementary NDT was performed using static step-frequency radar (SFR) combined to full-wave form inversion (FWFI) to estimate quantitatively the evolution of the saturated trench in the porous layer during the test.

This innovative technique promotes very-high frequency investigations, inducing high resolution [8], combined to calibrated waves propagation which can be fitted to an accurate forward model describing the complete signal. This methodology enables to retrieve the electromagnetic (EM) characteristics of the successive pavement layers [9].

After a presentation of the test site, the NDT techniques and the monitoring methodology are described. Then, results and discussion are developed in a following section.

II. POROUS PAVEMENT TEST SITE

A pavement structure has been constructed in Egletons (France) in order to validate experimentally heat exchanger function to retrieve solar energy in summer and to de-freeze road surface in winter (Fig. 1).

Pavement structure is composed of three layers (Fig. 2): a wearing course layer of semi-phaneritic asphalt concrete 6 cm thick (WL); a bonding course layer of 0/14 porous asphalt 8 cm thick (PAL) and a base layer of asphalt concrete with a thickness of 5 cm (BL). Porous asphalt layer has a porosity of 20% through which circulates fluid (water) via gravitational flow under slant (2%) effect.

This slant creates a hydraulic head difference between upstream and downstream part pavement through which fluid circulates.

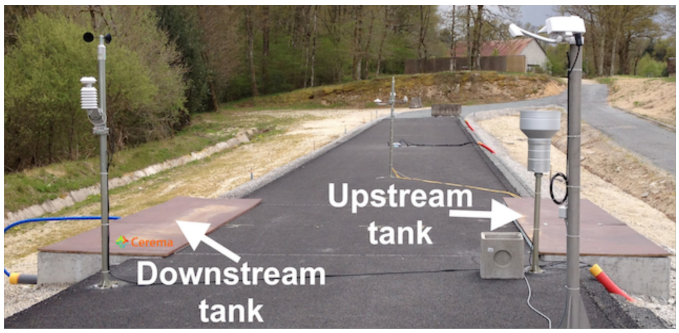

Fig. 1. Scheme of the porous pavement test site

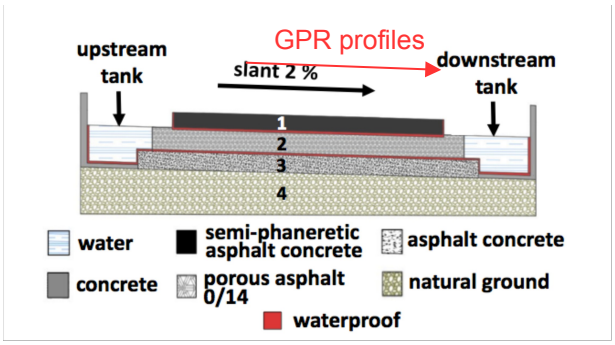

Fig. 2. Scheme of the pavement structure and orientation of GPR profiles

Two tanks, one upstream and one downstream, were constructed to supply and recover the fluid circulation in the drainage asphalt layer. Fluid circulation was maintained by a watertight seal between porous asphalt course and underlying layer. A pump is used to control different hydraulic heads losses between upstream and downstream tanks (fluid levels in the tanks). Different hydraulic regimes are achieved with varying pump's powers. In order to develop hydrothermal models for such pavement, we need to verify for example the saturated porous layer assumption when water level in each tank is at the top of the porous layer, objective of this paper.

III. Non-Destructive Monitoring Techniques

A. GPR technique

Two commercial impulse GPR system (SIR3000 from GSSI) were used in parallel, associated to ground-coupled 2.6 GHz antennas. The setting parameters were: a time range of 10 ns, a 512 sampling for A-scans, a frequency-band filtering [500 MHz – 5 GHz], a constant time gain (-6 dB) and spatial sampling of 1 cm.

Figure 3 presents an example of GPR B-scan performed at T0 before the beginning of water imbibition, and showing the pavement structure (Fig. 2). The two first interfaces, “Wearing Layer/Porous Asphalt Layer” (WL/PAL) and “Porous Asphalt Layer/Base Layer” (PAL/BL), are clearly visible at about 1 and 2.2 ns respectively, due high EM contrasts. It can be noted that the Base Layer, above unbound material, was laid in two times (slight visible interfaces at 3 and 3.4-3.6 ns).

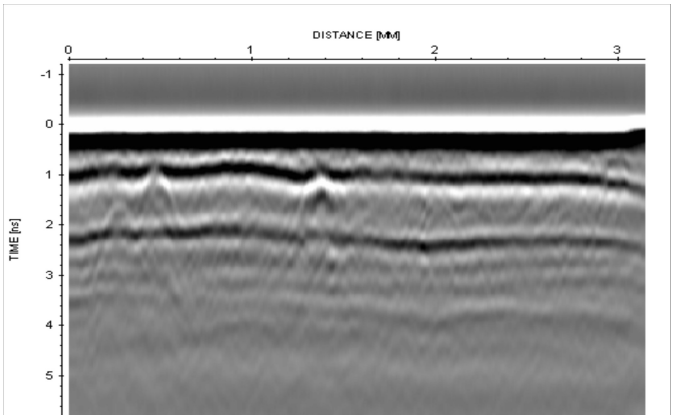

Fig. 3. Example of 2.6 GHz GPR B-scan, done on Line 3 on the structure before water imbibition process.

B. SFR technique

The second NDT method consists in a homemade stepped-frequency radar (SFR) system with an ultra-wide band (UWB) antenna [0.8 – 3 GHz] used in the near field conditions (at 4 cm from the pavement structure surface. For this experiment, SFR measurements were performed in a static mode, between Lines 6 and 7 at the abscissa 60 cm.

The radar full-waveform model of Lambot et al. [10, 11] is used to describe the wave/multi-layered medium interaction. This model is based on planar layered media Green’s functions combined with an intrinsic representation of the antenna through global reflection and transmission functions to account for antenna effects, including antenna-medium coupling. The pavement structure is considered as a three-layered dispersive medium, as shown in Fig. 4.

The considered transceiver is a mono-static SFR, which enables it to achieve high effective bandwidth with plural narrow instantaneous bandwidths. The dispersion of the materials is described by Jonscher’s model, which has shown the good performance for describing the frequency dependence of the effective permittivity [12]. To simplify the computation and the measurement configuration of the model, the distribution of the near field is assumed to be constant with a single point transceiver, where the antenna height is 4 cm over the studied medium. This model has been validated numerically and experimentally by [13].

The generalized model is described as the radar data S_{11}, the ratio of reflected and emitted EM waves, and can be given by the following equation [10, 11]:

$$S_{11}(f)=R_i(f)+T_i(f)\left(1-G(f)R_s(f)\right)^{-1}G(f)T_s(f) \quad (1)$$

where, R_i is the free space response of the antenna. T_i and T_s are the global transmission coefficients of the antenna for fields incident from the radar reference plane onto the source point and vice-versa, respectively. R_s is the global reflection coefficients for fields incident from the field point onto the radar reference plane. G is the spatial domain Green’s function, deduced from the zero-offset source-receiver Green function in the spectral domain.

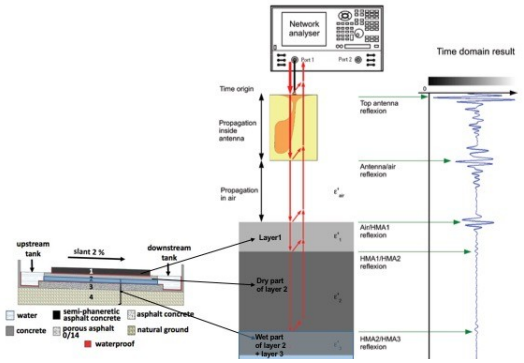

Fig. 4. Static configuration of SFR on the pavement test site

The objective of the inversion process is to reach the best set of model parameters which minimizes the difference between analytical radar data S_{11}^{mod} and the reference data S_{11}^{ref} (experimental data in the case of this study). Since the Jonscher's model has been chosen for the multi-layered pavement structure, the model parameters (integrated in the Green's function) include reference susceptibility χ_r, loss exponent n, instantaneous dielectric response ε_∞, direct-current conductivity σ_{dc} and the thickness of each layer of the modeled pavement structure. The solution is achieved by minimizing the objective function, which is weighted by a factor of amplitude:

$$O(m)=\frac{1}{NF}\sum_{i=1}^{NF}\frac{|S_{11}^{mod}(f_i,m)-S_{11}^{ref}(f_i)|}{|S_{11}^{ref}(f_i)|} \quad (2)$$

where $S_{11}^{mod}(f_i,m)$ and $S_{11}^{ref}(f_i)$ are the analytical and reference radar data S_{11} at the frequency point f_i, m is the model parameter, NF is the number of frequency points.

The studied geometry examined induces a total of 15 model parameters in the analytical model: χ_r, n, ε_∞, σ_{dc} and h of each layer.

Due to the fact that the medium below the dry porous asphalt during imbibition experiment is a very dispersive layer which contains water, natural ground, etc., all the entire medium below is simply considered as a virtual equivalent dispersive layer. The water penetrating depth is estimated by inversion of SFR data at all the test time points during the imbibition process.

The inversion procedure is therefore done in two steps: First, in the dry state T0, all the layer thicknesses are considered as known and the inversion of the SFR signals determines the 12 dielectric parameters of the Jonscher's model. The second step of the inversion fixes all inverted parameters during the first step and determines only the thickness of the dry porous asphalt layer. This thickness (theoretically from 8 cm to 0 cm) is inversely proportional to the water front height into the layer 2 (theoretically from 0 cm to 8 cm).

The genetic algorithm is adapted to the full-waveform inversion in this paper. It starts with an initial generation of candidate solutions that are tested against the objective function. In the case of this paper, a random initial generation with a population size of 50 individuals is used. The genetic algorithm generates the next generation after the selection, crossover and mutation processes of the current generation. The objective of this algorithm is to minimize the average value of all the objective functions in current generation. When the average change of best objective function over 5 generations is less than 0.001, or when a maximum generation of 100 is reached, the genetic algorithm stops and returns the inversion results.

C. *Monitoring methodology*

In order to accurately monitor the water ingress and transfer through the porous asphalt layer, 9 transversal Lines, in the direction of the gravity slope and distant laterally of 3m, were periodically surveyed by GPR.

Every 7 minutes, one GPR system surveyed from Line 0 to Line 4, while the second GPR system did the same from Line 8 to Line 5. This sequence lasted about 3 minutes. After an initial series of acquisition the water circulation is started from the upstream tank inside the porous asphalt layer. The saturated steady state was considered as established after one hour and half, leading to 18 series of GPR measurements in 115 minutes.

In parallel, SFR measurements were performed without stopping during every series, leading to huge amount of data and allowing possible averaging or accurate processing.

IV. GPR RESULTS AND DISCUSSION

Figure 5 presents a representative B-scan during the water imbibition process, showing the water front between about 1.6 and 2.2 m, which move towards the left with time.

While using this high central frequency, scattering on aggregates induce multiple reflexions in the B-scan, mainly visible in the saturated porous asphalt layer. Thus, the level of scattering imposes a picking process on the main amplitudes of the layers: black polarity of WL/PAL interface and white polarity of the water front.

The location of the water front becomes ambiguous while rising the wearing layer. The interaction merging the two elementary echoes induces shifts and amplitude modification while picking both interfaces. This effect is visible in Fig. 6, on the left part, the porous asphalt layer being roughly saturated.

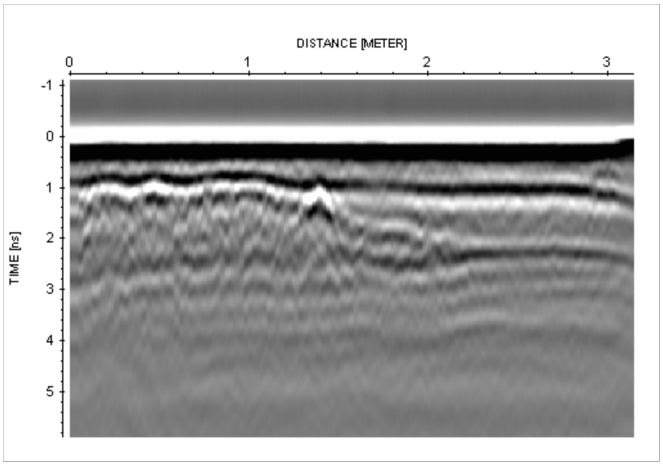

Fig. 5. GPR B-scan, done on Line 3 at the series T3 (16' of imbibition)

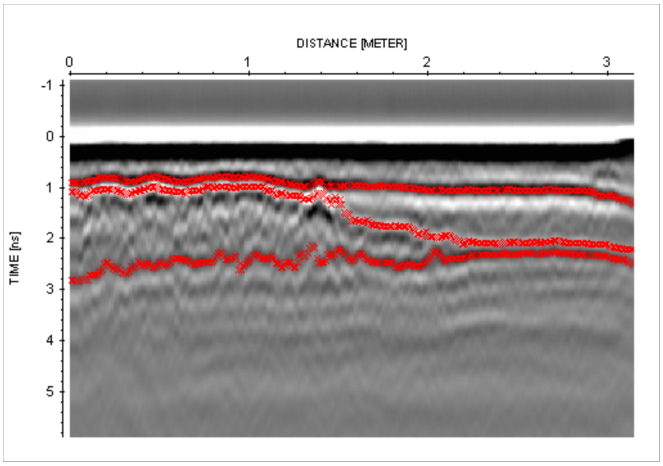

Fig. 6. GPR B-scan, from Fig.3, during the picking process

The two following picked layers present a logical half-wavelength decay. Nevertheless, the physical interaction merging the two elementary echoes induce major problem to pick the right polarity – and the right location – in the transition zones (about 1.4 and 2.2 m for the case of Fig.6).

The phenomenon is similar to the third picked layer as the first arrival (white polarity) is not visible on the bottom of saturated part on the left of Fig.6. Similarly, a half-wavelength decay has to be taken into account.

While gathering the picking values of WL/PAL interface (black polarity) during the monitoring (Fig. 7), one can see a shift on the left part due to the apparent saturation of the PAL. Nevertheless, this effect remain non visible after 1.4 m. At this specific location, the presence of a thermal sensor, combined with the topography at this interface, can explain the double behavior creating a captive air lens.

This shift on the first 1.4 m is confirmed on Fig. 8 while picking the water front (white polarity). The water flow is visible from the eleventh minutes, going through the structure in less than 40 minutes. Moreover, results show that the complete saturation of the PAL is not reached in steady state on the last meter.

The monitoring of the water front is summarized in Fig. 8 showing the velocity of the fluid transfer. The water flow joins the opposite side of the road in about 24' (between T4 and T5).

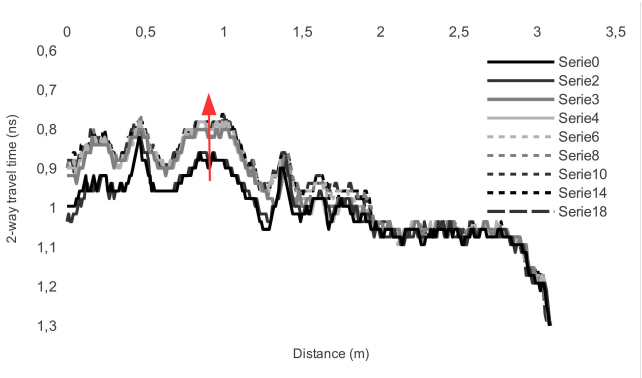

Fig. 7. Time picking of interface WL/PAL for different series done on Line3

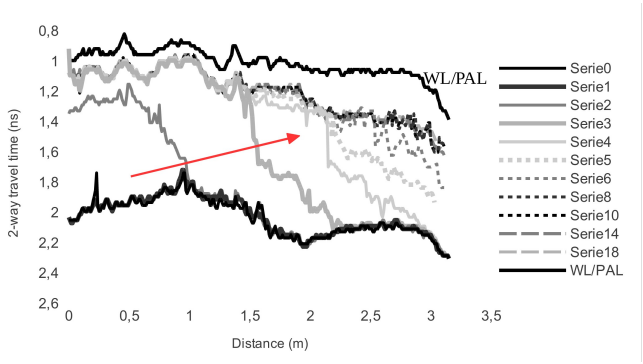

Fig. 8. Time picking of the water front flowing in PAL for different series done on Line3. WL/PAL black curve corresponds to serie0 for reminder

Then the right part of the structure is filled with water. Nevertheless, one can see that an air lens, from 1.5 to 3.2 m, remains in steady state (visible after series T8), as the difference of polarity peaked does not explain the decay between WL/PAL and the water front.

Figs 9 and 10 present GPR Bscans at different times (T3 and T4) performed on Line 6, near the SFR static monitoring. These profiles precise the time range to be studied as a priority.

While detailing Fig. 11, we note two water-flow behaviors: a sharp water front associated to a PAL nearly saturated in the two first meters, and a horizontal water filling in the second part of the structure.

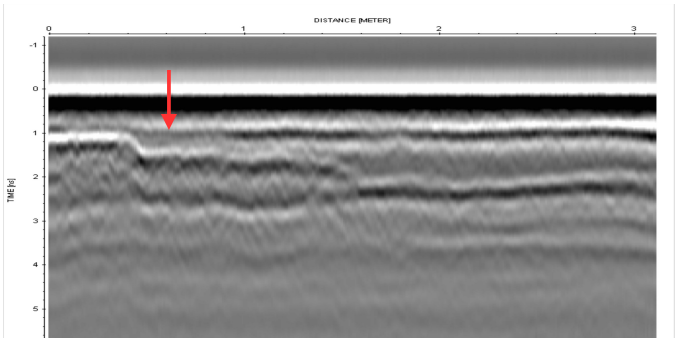

Fig. 9. GPR B-scan, done on Line6 at the series T3 (16' of imbibition). The red arrow shows the location of the SFR measurements

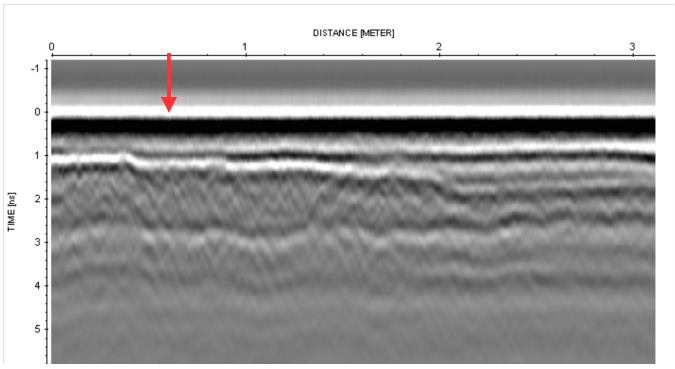

Fig. 10. GPR B-scan, done on Line 6 at the series T4 (22' of imbibition)

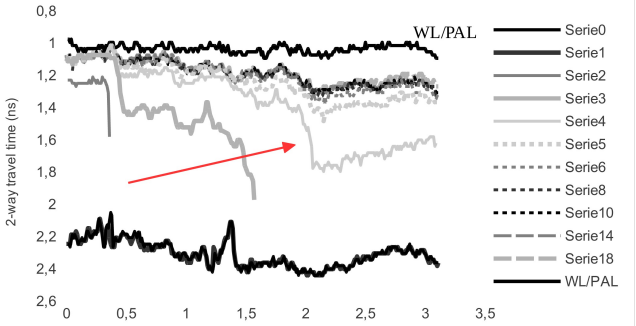

Fig. 11. Time picking of the water front flowing in PAL for different series done on Line6

Moreover, one can see that an air lens, from 2 to 3.2 m, remains in steady state (visible after series T6). This air lens is linked upstream with a slight widening air beam in the first part, while studying the decay between WL/PAL and the water front.

These different behaviors could be explained by the vertical topology of the upper watertight interface which is not known.

V. SFR RESULTS AND DISCUSSION

The SFR inversion process is detailed for the initial test time (T0) as example. The objective function gives a minimal value of 0.052, which indicates that the correspondence is efficient in the frequency domain. The correspondence between analytical and experimental radar data when the inversion ends is shown in Fig. 12.

It should be noticed that the small differences are due to the assumption of the so called "equivalent layer". It should be also be mentioned that, the reflections in the time domain signal in Fig. 12c are very hard to be distinguished,, as they are mixed with each other. In this case, it is not possible to use the usual amplitude inversion in the time domain. But full-waveform inversion of the frequency domain signal is powerful in such a case. This inversion method returns a global minimum, as shown in Fig. 13.

The inversion results of the experimental radar data, which shows the inverted Jonscher's model parameters of the pavement structure layers, can be seen in Table 1 (and in Fig. 14 in terms of complex permittivities of each layer).

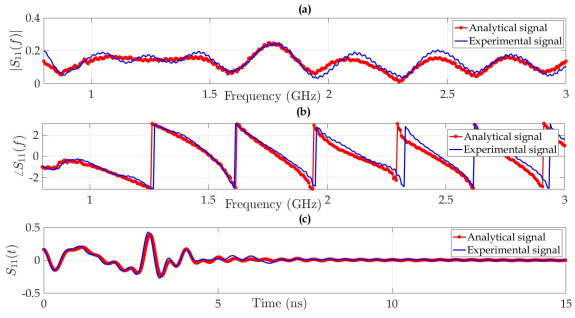

Fig. 12. Comparison between analytical and experimental signals, $S_{11}^{mod}(f_i,m)$ and $S_{11}^{ref}(f_i)$, when inversion ends

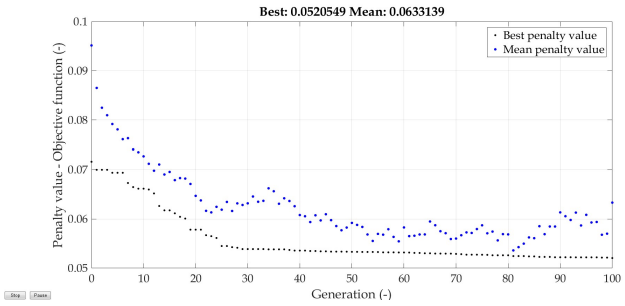

Fig. 13. Evolution of the objective function vs. iteration

It is necessary to note that these results are obtained in the initial dry state T0 where the thicknesses of each layer are well known. These inverted parameters (Table 1) will be considered in the rest of the experimental/inversion process as invariables (inversion input) and the inversion output will be then limited to the thickness of the dry porous asphalt layer (dry part of layer 2), which is a strong hypothesis.

The direct measurement at a static point shows the penetration tendency of the water into the material (Fig. 17). Indeed, we can follow (as for GSSI measurements) the reflection on the water front into layer 2. However, the temporal picking gives an indication of the evolution of the water front but not of its exact position. We thus carried out inversions of the SFR signals on the times T0, T1, T3, T4, T5, T6, T12, T17 and T21 (T0 + 7', T0 + 20', T0 + 27', T0 + 34', T0 + 40', T0 + 70', T0 + 98' and T0 + 130' respectively) for the estimation of the thicknesses of the dry PAL (dry part of layer 2). The results of the inverted thicknesses as a function of the imbibition times are shown in Fig. 15.

We can see in the results of this figure that the water penetration front does not theoretically reach the interface between the layers 1 and 2. In other words, the water only penetrates into the draining layer until a maximum height of 6 cm instead of the targeted 8 cm.

However, these results can be biased by the different water gradients at this position of the pavement structure. Indeed, the slant at this measurement point is in two directions, which explains by the way the results of the GPR measurements on Line 6.

Another explanation for this shift can be associated with the initial hydric state of the pavement structure. Indeed, at the T0 of the experiment, a water purge was performed but was not really confirmed. This uncertainty could lead to a biased estimation of Jonscher's parameters in the initial state for which the associated initial value of 8 cm of the thickness of layer 2 is not realistic.

TABLE I. TABLE

Layer	χ_r	n	ε_∞	σ_{dc}	H (known) (m)
Layer 1	3.5	1.0	0.9	0.002	6.5
Layer 2 (PAL)	2.7	0.94	0.0	0.000	8
Virtual equivalent layer "3" (3+4+...)	2.9	0.98	0.6	0.020	∞

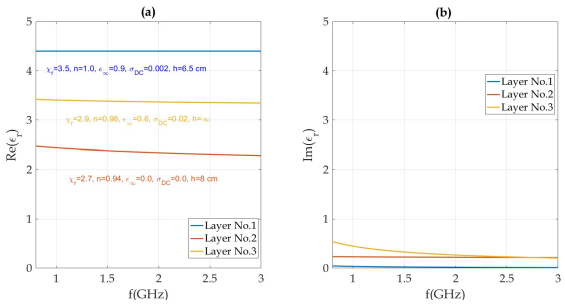

Fig. 14. Inversed effective permittivities of the three considered layers

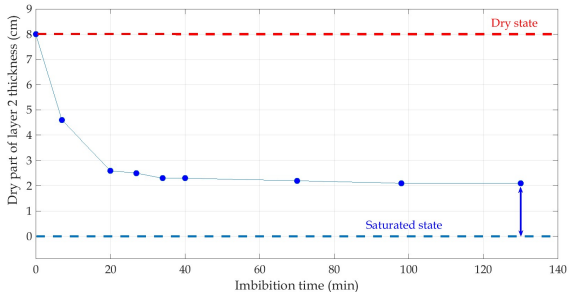

Fig. 15. Evolution of the estimated dry thickness of the PAL during the monitoring.

The last explanation, which goes against the previous one, can come from the hypothesis of the constant EM nature of the third equivalent layer (fixed for every inversion). The water flow could induce a non negligible bias in the fixed values defining the layer "3" and then induce a bias in the estimation of the dry thickness.

Even if the accuracy of the estimated values of thickness could be discussed, the monitoring experiment has shown the efficiency of the studied NDT methodology.

VI. Conclusion

The monitoring of a water imbibition of a particular porous pavement structure has been performed using GPR and SFR techniques. GPR measurements were able to follow the water front progress while peaking the double travel times. In parallel, static SFR measurements were continuously done and inverted using a FWI technique in the frequency domain.

GPR results can follow the water front and show different behaviors of the water transfer in the PAL, which could be explained by the vertical topology of the upper watertight interface. SFR results show similar results to GPR, while giving quantitative information on the height of the water front inside the PAL.

Then, the GPR and SFR methodology has been validated for the monitoring of water transfer in special porous pavement structure.

References

[1] P. Pan, S. Wu, Y. Xiao, G. Liu, "A review on hydronic asphalt pavement for energy harvesting and snow melting", Renew. Sustain. Energy Rev. 48, 2015, pp. XX.

[2] S. Andriopoulou, "A Review on Energy Harvesting From Roads", KTH, 2012.

[3] V. Bobes-Jesus, P. Pascual-Muñoz, D. Castro-Fresno, J. Rodriguez-Hernandez, "Asphalt solar collectors: a literature review", Appl. Energy, vol. 102, 2013.

[4] S. Asfour, F. Bernardin, E. Toussain, J.M. Piau, "Hydrothermal modeling of porous pavement for its surface de-freezing", Appl. Therm. Eng., vol. 2, 2016, pp. 493-500.

[5] W.L Lai., X. Dérobert, A.P. Annan, "A review of Ground Penetrating Radar Application in Civil Engineering: a 30-year journey from Locating, Testing and Evaluation to Imaging and Diagnosis", NDT&E Int., spec. issue, (in press), 2017. 10.1016/j.ndteint.2017.04.002

[6] T. Saarenketo, T. Scullion, "Road evaluation with ground penetrating radar", J. Appl. Geophys., vol. 43, 2000, pp. 119-139.

[7] A. Loizos, C. Plati, "Accuracy of pavement thicknesses estimation using different ground penetrating radar analysis approaches", NDT&E Int., vol. 40, 2007, pp. 147-157.

[8] X. Dérobert, C. Fauchard, Ph. Côte, E. Le Brusq, E. Guillanton, J.Y. Dauvignac, Ch. Pichot, "Step frequency radar applied on thin road layers", J. Appl. Geophys., vol. 47, 2001, pp. 317-325.

[9] B. Guan., A. Ihamouten, X. Dérobert, S. Lambot, G. Villain, "Near-field full-waveform inversion of radar waves to monitor water front in limestone", Journ. Selec. Top. Appl. Earth Obs. & Remote Sens., Vol. 99, 2017, pp. 1-9.

[10] S. Lambot, E. Slob, I. Van den Bosch, B. Stockbroeckx, M. Vanclooster, "Modeling of ground-penetrating radar for accurate characterization of subsurface electric properties", IEEE Trans. Geosci. & Remote Sens., vol. 42, 2004, pp. 2555-2568.

[11] S. Lambot S and F. Andre F, "Full-wave modeling of near-field radar data for planar layered media reconstruction", IEEE Trans. Geosci. & Remote Sens., vol. 52, 2014, pp. 2295-2303.

[12] A. Ihamouten, K. Chahine, V. Baltazart, G. Villain, X. Dérobert "On variants of the frequency power law for the electromagnetic characterization of hydraulic concrete", IEEE Trans. Instrum. Meas., vol. 60, 2011, pp. 3658-3668.

[13] B. Guan, A. Ihamouten, X. Dérobert, S. Lambot, G. Villain, "Near-field full-waveform inversion of radar waves to monitor water front in limestone", Journ. Selec. Top. Appl. Earth Obs. & Remote Sens., vol. 99, 2017, pp. 1-9.